

Electronic Supplementary Information

Tetradentate Schiff base platinum(II) complexes as new class of phosphorescent materials for high-efficiency and white-light electroluminescent devices

Chi-Ming Che,^{*a} Siu-Chung Chan,^a Hai-Feng Xiang,^a Michael C. W. Chan,^a Yu Liu^b and Yue Wang^b

^a *Department of Chemistry and HKU-CAS Joint Laboratory on New Materials, The University of Hong Kong, Pokfulam Road, Hong Kong, China. Fax: +852 2857 1586; E-mail: cmche@hku.hk*

^b *Key Laboratory for Supramolecular Structure and Spectroscopy of Ministry of Education, Jilin University, Changchun 130023, China.*

Synthesis and spectroscopic, thermal (TGA), photophysical, electrochemical and electroluminescent characterization.

Experimental Section

Materials and Instrumentation: All chemicals and solvents (AR grade) were used as received. The solvents for physical measurements were purified according to literature methods.¹ Elemental analyses were performed by the Institute of Chemistry at Chinese Academy of Sciences, Beijing. ¹H and ¹³C NMR spectra were recorded on Bruker DPX-300 or 500 multinuclear FT-NMR spectrometers at 298 K using tetramethylsilane as the internal standard. Positive ion FAB and EI mass spectra were recorded on a Finnigan MAT95 mass spectrometer. Infrared spectra were obtained on a Bio-Rad FTs-165 spectrometer in KBr.

Photophysical studies: UV-visible absorption spectra were obtained on a Hewlett Packard 8453 UV/VIS spectrophotometer. Steady state emission and excitation spectra at 298 and 77 K were obtained on a Spex 1681 Fluorolog-2 Model F111 spectrophotometer equipped with a Hamamatsu R928 PMT detector. The 77 K solid-state and glassy [EtOH/MeOH (4:1 v/v)] emission and excitation spectra were recorded with the sample loaded in a quartz tube inside a quartz-walled optical Dewar flask filled with liquid nitrogen. All solutions for photophysical measurements were degassed in a high-vacuum line for at least four freeze-pump-thaw cycles. Emission lifetimes were measured with a Quanta-Ray Q-switch DCR-3 Nd:YAG pulsed laser system (pulse output 355 nm, 8 ns).

Emission quantum yields were measured by the method of Demas and Crosby² using a degassed acetonitrile solution of [Ru(bpy)₃]Cl₂ (bpy = 2,2'-bipyridine) as the standard ($\Phi_r = 0.062$). Calculations were carried out using the equation $\Phi_s = \Phi_r(B_r/B_s)(n_s/n_r)^2(D_s/D_r)$, where the subscripts s and r refer to the sample and reference standard solution respectively, n is the refractive index of the solvents, D is the integrated intensity, and Φ is the luminescence quantum yield. The quantity B is calculated from $B = 1 - 10^{-AL}$, where A is the absorbance at the excitation wavelength and L is the optical path length. Errors for λ (± 1 nm), τ (± 10 %), and Φ (± 10 %) values are estimated.

Cyclic voltammetry: Cyclic voltammetry was performed using a PAR potentiostat/galvanostat model 273A with the PowerSuite 2.12.1 program at a scan rate of 50 mV s⁻¹. Electrochemical measurements were performed at room temperature after purging with nitrogen using 0.1 M tetrabutylammonium hexafluorophosphate (TBAP)/acetonitrile (or DMF) as the supporting electrolyte. The working electrode was a glassy carbon (geometric

area of 0.02 cm²) electrode and the counter electrode was platinum gauze. A non-aqueous Ag/AgNO₃ (0.1 M in acetonitrile) reference electrode was contained in a separate compartment connected to the test solution via fine sintered glass disks. The ferrocenium/ferrocene couple was added and used as the internal standard.

From the electrochemical data, the excited-state potential of **1** can be estimated using equation 1:

$$E^\circ(\mathbf{1}^+/\mathbf{1}^*) = E^\circ(\mathbf{1}^+/\mathbf{1}) - E_{0-0} \quad (1)$$

The E_{0-0} estimated from the emission spectrum is 2.51 eV (495 nm) and the $E^\circ(\mathbf{1}^+/\mathbf{1})$ is ≤ 0.60 V versus FeCp₂⁺⁰ (i.e. ≤ 0.91 V versus SSCE). Hence, the excited-state potential of **1*** is ≤ -1.6 V versus SSCE. However, the irreversible nature of the electrochemical waves means that the excited-state reduction potential estimated in this manner is not precise.

The quenching of **1*** by a series of pyridinium acceptors³ in acetonitrile has been studied. The bimolecular rate constants (k_q) are summarized in Table S3. The large negative values indicate that the quenching processes are largely diffusion controlled, and hence corrected quenching rate constants (k_q') are calculated. Using the Rehm-Weller equation, the plot of $\ln k_q'$ versus $E^\circ(A^+/A)$ gave the excited-state potential $E^\circ(\mathbf{1}^+/\mathbf{1}^*)$ of -1.75 V versus SSCE. This value is consistent with the estimated value of ≤ -1.6 V versus SSCE obtained from equation 1 using electrochemical and spectroscopic data.

Synthesis: [Pt(L¹)] (1). The synthetic procedure was modified from a published method⁴ containing characterization by elemental analysis. K₂PtCl₄ (0.31 g, 0.75 mmol) was added to an aqueous KOH solution (1 M, 20 ml) containing H₂L¹ (*N,N'*-bis(salicylidene)-1,2-ethylenediamine; 0.20 g, 0.75 mmol), and the mixture was stirred and heated at 40 °C for 8 hours under argon. The resultant precipitate was filtered and washed with KOH (1 M, 2 × 20 ml) and water. The solid was dried and purified by silica gel chromatography using dichloromethane as the eluent. The product was eluted as a yellow band which was evaporated to dryness. The yellow solid was recrystallized by slow evaporation of an acetonitrile solution to give orange crystals. Yield: 50 % (0.17 g). ¹H NMR (DMSO-d₆): δ = 8.55 (s, 2H, HC=N), 7.51 (dd, J = 7.9, 1.7 Hz, 2H, Ph), 7.44 (td, J = 7.2, 1.8 Hz, 2H, Ph), 6.91 (d, J = 8.4 Hz, 2H, Ph), 6.62 (td, J = 7.4, 1.0 Hz, 2H, Ph), 3.83 (s, 4H, CH₂). ¹³C NMR (DMSO-d₆): δ = 162.5, 156.0, 133.7, 133.5, 122.3, 121.0, 115.5, 61.0. MS-FAB⁺ (*m*-NBA): m/z : 461 [M]⁺. IR (KBr): ν = 3075, 3044, 3021, 3012, 1624, 1601, 1534 cm⁻¹. Anal. Calcd (%) for C₁₆H₁₄N₂O₂Pt: C, 41.65; H, 3.06; N, 6.07. Found: C, 41.67; H, 3.09; N, 6.11.

[Pt(L²)] (2). The synthetic procedure was similar to that for **1** except H₂L² (*N,N'*-bis(salicylidene)-1,3-propanediamine; 0.21 g, 0.75 mmol) was used. The resultant yellow brown precipitate was collected and purified on a silica gel column using dichloromethane/ethyl acetate (10:1) as eluent. Orange crystals were obtained by slow evaporation of an acetonitrile solution. Yield: 21 % (75 mg). ¹H NMR (CDCl₃): δ = 7.75 (s, 2H, HC=N), 7.41 (td, *J* = 7.7, 1.7 Hz, 2H, Ph), 7.15–7.10 (m, 4H, Ph), 6.57 (t, *J* = 7.4 Hz, 2H, Ph), 3.91 (m, 4H, NCH₂), 2.12 (pentet, *J* = 5.1 Hz, 2H, NCH₂CH₂). ¹³C NMR (CDCl₃): δ = 162.6, 158.8, 134.2, 133.2, 120.9, 120.0, 115.7, 62.1, 29.7. MS-FAB⁺ (*m*-NBA): *m/z*: 475 [M]⁺. IR (KBr): ν = 3059, 3031, 2943, 2919, 1611, 1542 cm⁻¹. Anal. Calcd (%) for C₁₇H₁₆Br₄N₂O₂Pt: C, 42.95; H, 3.39; N, 5.89. Found: C, 42.70; H, 3.40; N, 5.88.

[Pt(L³)] (3). The procedure was similar to that for **1**, except H₂L³ (*N,N'*-bis(salicylidene)-1,1,2,2-tetramethylethylenediamine; 0.24 g, 0.75 mmol) was used. The yellow residue was purified on a silica gel column using dichloromethane as eluent and recrystallized by slow evaporation of an acetonitrile solution. Yield: 40 % (0.16 g). ¹H NMR (CDCl₃): δ = 8.16 (s, 2H, HC=N), 7.46 (td, *J* = 7.7, 1.8 Hz, 2H, Ph), 7.35 (dd, *J* = 7.9, 1.7 Hz, 2H, Ph), 7.25 (d, *J* = 7.2 Hz, 2H, Ph), 6.63 (t, *J* = 6.9 Hz, 2H, Ph), 1.53 (s, 12H, Me). ¹³C NMR (CDCl₃): δ = 163.6, 151.8, 134.0, 133.5, 122.8, 122.3, 116.0, 75.9, 24.7. MS-FAB⁺ (*m*-NBA): *m/z*: 517 [M]⁺. IR (KBr): ν = 3046, 3017, 2983, 2928, 1611, 1600, 1535 cm⁻¹. Anal. Calcd (%) for C₂₀H₂₂N₂O₂Pt: C, 46.42; H, 4.29; N, 5.41. Found: C, 46.08; H, 4.27; N, 5.25.

X-ray crystallography: Crystal data: C₂₀H₂₂N₂O₂Pt, *M* = 517.49, crystal size = 0.3 × 0.2 × 0.1 mm, monoclinic, *P*2₁/*c*, *a* = 22.384(5) Å, *b* = 20.718(4) Å, *c* = 12.077(2) Å, β = 94.90(3)°, *V* = 5580(2) Å³, *Z* = 12, *D*_c = 1.848 g cm⁻³, μ(MoKα) = 7.558 mm⁻¹, *F*(000) = 3000, *T* = 253(2) K, 2θ_{max} = 50.7°, 9009 independent reflections (*R*_{int} = 0.069), 658 variable parameters, *R*₁ = 0.039, *wR*₂ = 0.081, GOF(*F*²) = 0.788, max./min. residual electron density 0.960/−2.327 eÅ⁻³. Data collection was performed on a MAR diffractometer with a 300 mm image plate detector using graphite monochromatized MoKα radiation [λ(MoKα) = 0.71073 Å].

Electroluminescence: The ITO coated glass slide was cleaned successively with toluene, acetone, methanol and deionized water in ultrasonic bath for 10 minutes using each solvent. It

was then dried in an infrared oven and stored in analytical grade acetone. The cleaned glass slide was treated in boiling H₂O₂ (50 %) for 10 minutes, dried in an IR oven and followed by ultraviolet cleaner before use.

For devices containing complex **1** as dopant, each device was assembled in the following sequence: indium tin oxide (ITO) with sheet resistance of 20 Ω/square on glass substrate (anode); 500 Å of α-naphthylphenylbiphenyl amine (NPB; hole-transport material); 500 Å of the emitting layer, made of bis(2(2'-hydroxyphenyl)pyridine)beryllium⁵ (Bepp₂; host) and complex **1** (dopant); 15 Å of lithium fluoride (LiF; electron-injection layer); 2500 Å of aluminum (cathode). For devices containing complex **3** as dopant, each device was assembled in the following sequence: ITO on glass substrate (anode); 400 Å of NPB; 300 Å of the emitting layer, consisting of 4,4'-(N,N'-dicarbazole)biphenyl (CBP; host) and complex **3** (dopant); 200 Å of 2,9-dimethyl-4,7-diphenyl-1,10-phenanthroline (BCP; hole-blocking material); 300 Å of Alq₃ (electron-transporting material); 5 Å of LiF; 1500 Å of aluminum (cathode).

The organic layers were laminated in the above sequence under 5×10^{-6} mbar without breaking vacuum between each vacuum deposition process. The cathode metal was deposited in another chamber under 5×10^{-6} mbar vacuum immediately after the organic layers were deposited. The organic layers were deposited at rates of 2 to 5 Å per second. The active area of each single device is 3 × 3 mm as defined by the overlapping area of the anode and the cathode. The EL spectra and current-voltage-luminance characteristics were recorded in air with a Spectroscan PR-650 spectrometer. The external quantum efficiencies η_{ext} were calculated based on the method described by Okamoto and coworkers⁶ using luminance, EL spectrum and current density.

-
- 1 D. D. Perrin, W. L. F. Armargo, D. R. Perrin, ed., *Purification of Laboratory Chemicals*, Pergamon Press, Oxford, 1983, 2nd Edition.
 - 2 J. N. Demas, G. A. Crosby, *J. Phys. Chem.*, 1971, **75**, 991–1024.
 - 3 J. L. Marshall, S. R. Stobart, H. B. Gray, *J. Am. Chem. Soc.*, 1984, **106**, 3027–3029.
 - 4 M. E. Ivanova, G. A. Shagisultanova, *Russ. J. Phys. Chem.*, 1991, **65**, 1563; L. P. Ardasheva, G. A. Shagisultanova, *Russ. J. Inorg. Chem.*, 1998, **43**, 85.
 - 5 a) Y. Liu, J. Guo, J. Feng, H. Zhang, Y. Li, Y. Wang, *Appl. Phys. Lett.*, 2001, **78**, 2300–2302; b) Y. Li, Y. Liu, W. Bu, D. Lu, Y. Wu, Y. Wang, *Chem. Mater.*, 2000, **12**, 2672–2675.
 - 6 S. Okamoto, K. Tanaka, Y. Izumi, H. Adachi, T. Yamaji, T. Suzuki, *Jpn. J. Appl. Phys.*, 2001, **40**, L783.

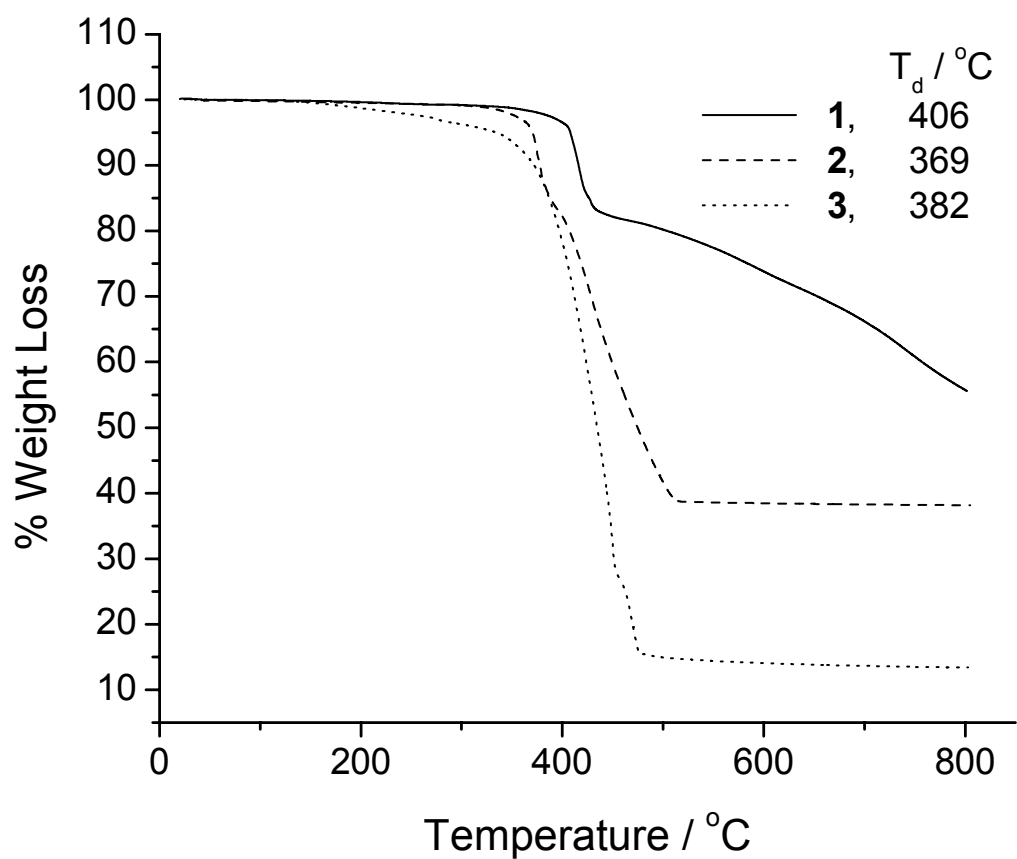


Figure S1. TGA thermograms of platinum Schiff base complexes (T_d = decomposition temperature).

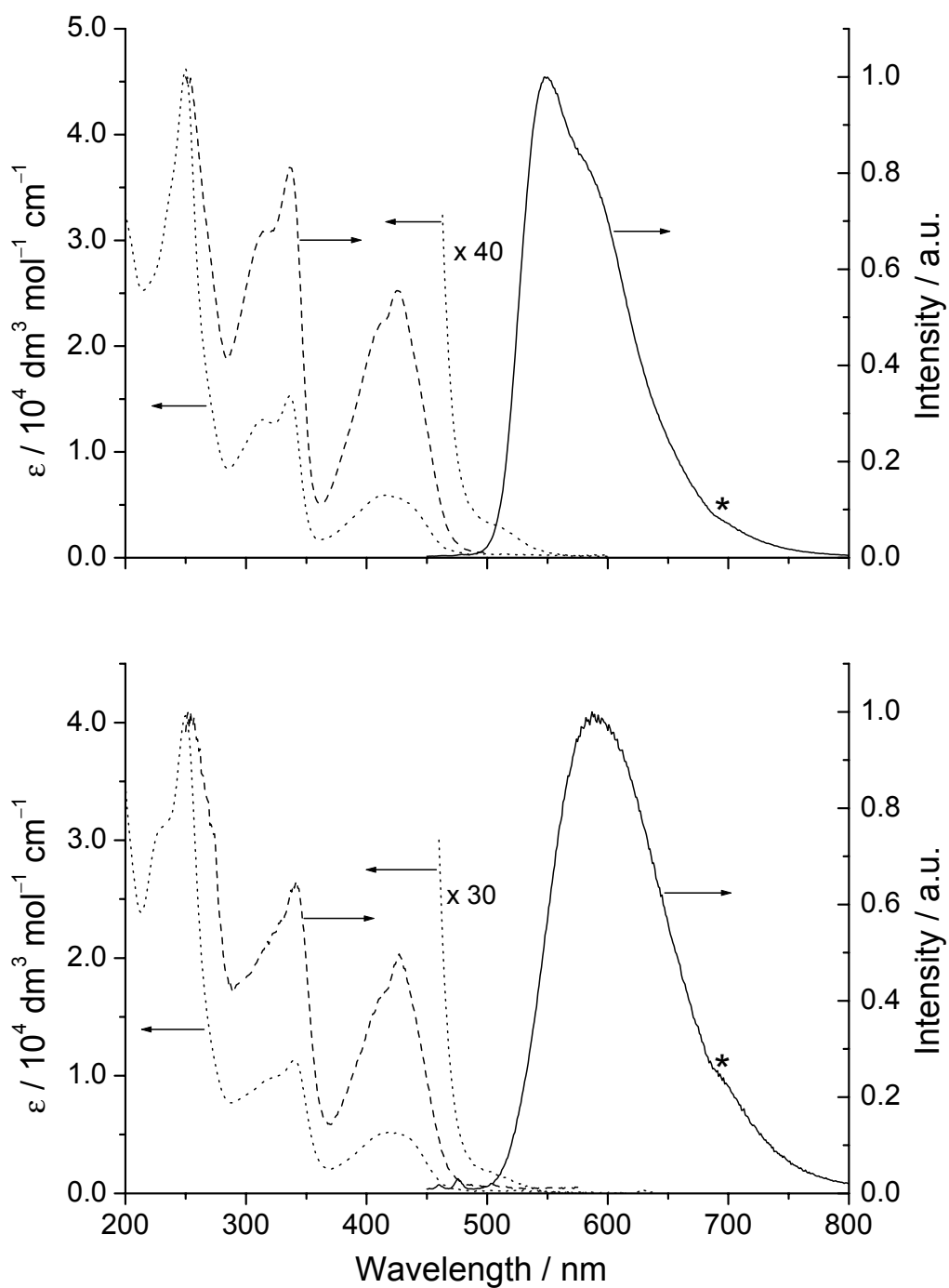


Figure S2. Absorption (dot), excitation (dash) and emission (solid; $\lambda_{\text{ex}} = 420 \text{ nm}$) spectra of **1** (top) and **2** (bottom) in acetonitrile at 298 K (* indicates artifact).

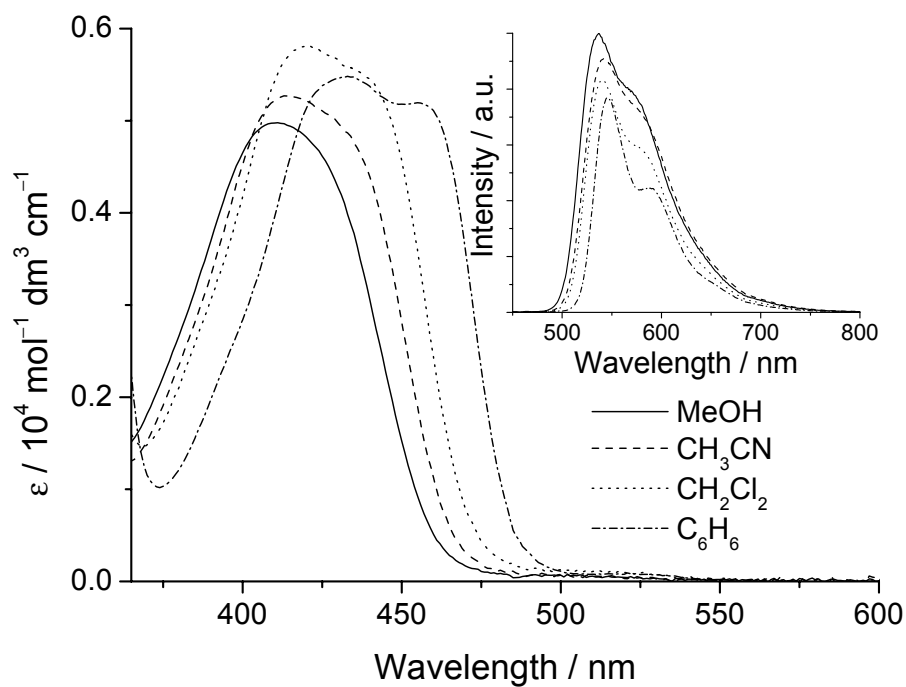


Figure S3. Absorption and emission (inset, $\lambda_{\text{ex}} = 420 \text{ nm}$) spectra of **3** (conc. $\approx 2 \times 10^{-5} \text{ M}$) in various solvents at 298 K.

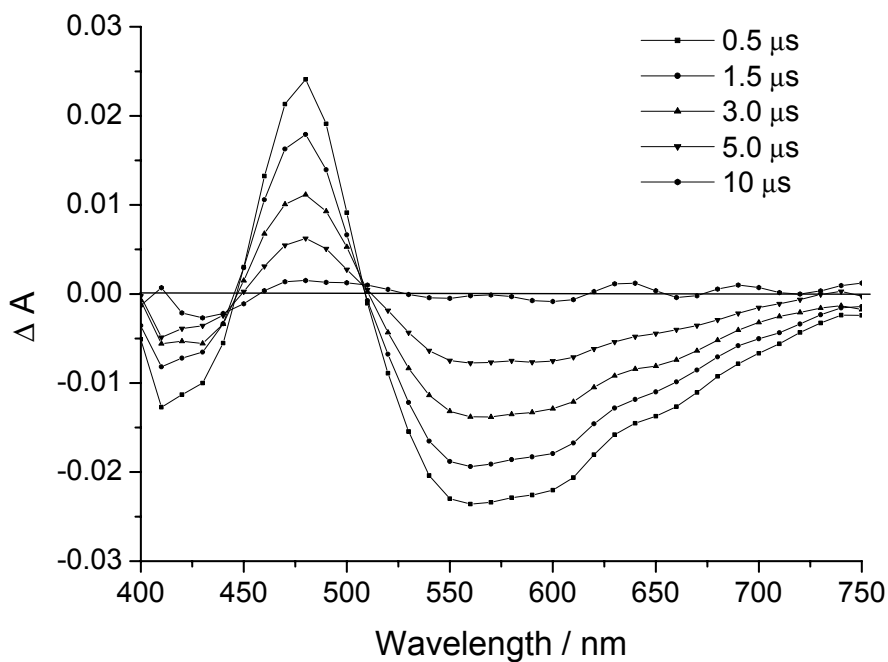


Figure S4. Time-resolved absorption difference spectra of **3** (conc. $= 2 \times 10^{-5} \text{ M}$) in degassed acetonitrile solution following 355 nm excitation at 298 K.

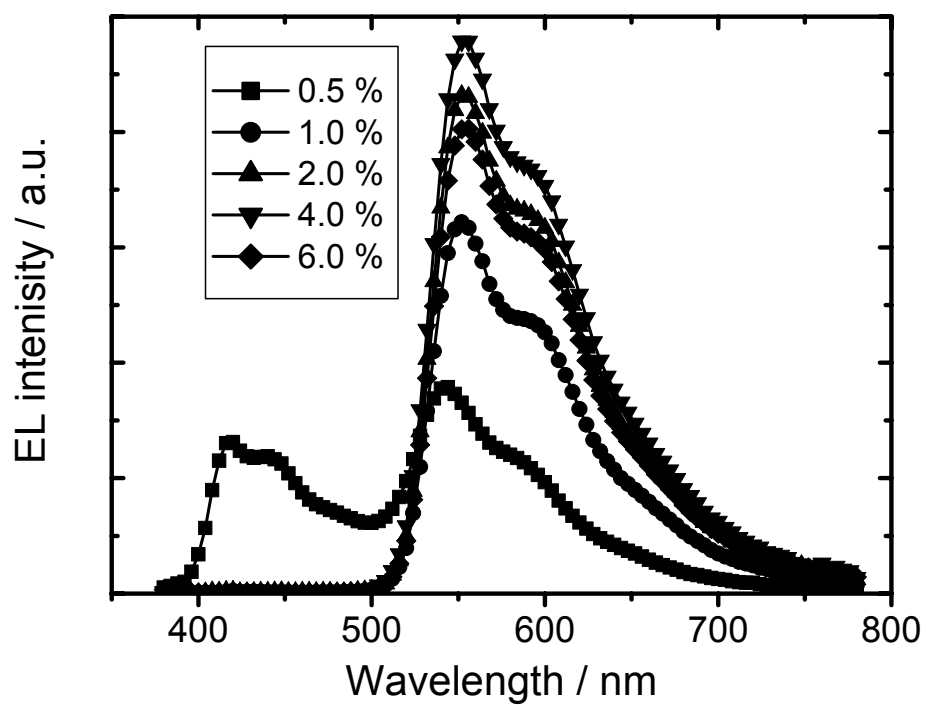


Figure S5. EL spectra of **3**-doped OLEDs at different dopant concentrations under applied voltage of 8 V.

Table S1. Photophysical data

Complex	Medium (<i>T</i> [K])	λ_{abs} [nm] (ϵ [$10^4 \text{ dm}^3 \text{ mol}^{-1} \text{ cm}^{-1}$])	λ_{em} [nm]	τ [μs] ^[a] (Φ_{em})	
[Pt(L ¹)] (1)	MeCN (298)	314 (1.30), 336 (1.53), 417 (0.59), 503 (sh, 0.008)	550 (max), 580 (sh)	3.5 (0.19)	
	solid (298)	-	548 (max), 594, 648 (sh)	0.2	
	solid (77)	-	564 (max), 619	3.0	
	EtOH:MeOH (77)	-	521 (max), 565, 615 (sh)	10.7	
[Pt(L ²)] (2)	MeCN (298)	230 (3.15), 250 (4.08), 320 (sh, 0.96), 340 (1.12), 420 (0.51), 500 (sh, 0.006)	592	0.5 (0.09)	
	solid (298)	-	598	_ [b]	
	solid (77)	-	612	0.7	
	EtOH:MeOH (77)	-	521 (max), 560	6.5	
[Pt(L ³)] (3)	MeOH (298)	317 (1.08), 337 (1.38), 411 (0.50), 430 (sh, 0.43), 492 (sh, 0.008)	537 (max), 570 (sh)	3.4 (0.17)	
	MeCN (298)	316 (1.16), 339 (1.42), 413 (0.53), 432 (sh, 0.48), 501 (0.006)	541 (max), 580 (sh)	3.4 (0.18)	
	CH ₂ Cl ₂ (298)	319 (1.31), 344 (1.67), 420 (0.58), 440 (0.54), 510 (0.008)	542 (max), 577 (sh)	3.7 (0.27)	
	C ₆ H ₆ (298)	323 (1.26), 351 (1.53), 433 (0.55), 455 (0.52), 521 (0.008)	546 (max), 588	3.9 (0.27)	
	solid (298)	-	551 (max), 585	1.5	
	solid (77)	-	544 (max), 589, 644	6.4	
	EtOH:MeOH (77)	-	514 (max), 555, 595	10	

[a] Lifetime was measured at peak maximum. [b] Lifetime cannot be detected due to weak emission.

Table S2. Ground- and excited-state redox potentials

Complex	E_{0-0} (eV)	E_{pa} (V) ^[a]	$E^\circ(\mathbf{Pt}^+/\mathbf{Pt}^*)$ ^[b]
1	2.51	0.60	-1.60
2	2.50	0.63	-1.56
3	2.56	0.65	-1.60

[a] Concentration $\sim 10^{-4}$ M, recorded in CH₃CN at 50 mV s⁻¹, 0.1 mol dm⁻³ [*n*Bu₄N][PF₆], referenced to FeCp₂⁺⁰. This value refers to the first anodic peak.

[b] Estimated by $E^\circ(\mathbf{Pt}^+/\mathbf{Pt}^*) = E^\circ(\mathbf{Pt}^+/\mathbf{Pt}) - E_{0-0}(\mathbf{Pt} = \mathbf{1}, \mathbf{2} \text{ or } \mathbf{3})$. Potential versus SSCE.

Table S3. Rate constants for quenching of **1*** by pyridinium acceptors in acetonitrile (0.1 mol dm⁻³ TBAP) at 25 °C.

Pyridinium salt ^[a]	$E^\circ(\mathbf{A}^+/\mathbf{A})$ ^[b] [V vs SSCE]	k_q [dm ³ mol ⁻¹ s ⁻¹]	k_q' ^[c] [dm ³ mol ⁻¹ s ⁻¹]	ln k_q'
<i>N,N'</i> -dimethyl-4,4'-bipyridinium	-0.45	1.2×10^{10}	3.0×10^{10}	24.13
4-amido- <i>N</i> -ethylpyridinium	-0.93	7.99×10^9	1.33×10^{10}	23.31
3-amido- <i>N</i> -benzylpyridinium	-1.07	6.6×10^9	9.85×10^9	23.01
3-amido- <i>N</i> -methylpyridinium	-1.14	6.14×10^9	8.86×10^9	22.90
2,6-dimethyl- <i>N</i> -methylpyridinium	-1.52	9.1×10^7	9.14×10^7	18.33
2,4,6-trimethyl- <i>N</i> -methylpyridinium	-1.67	1.13×10^7	1.13×10^7	16.24

[a] All quenchers are hexafluorophosphate salts. [b] Reference 3. [c] $(1/k_q') = (1/k_q) - (1/k_d)$, where k_d is the diffusion-limited rate constant, taken to be 2×10^{10} dm³ mol⁻¹ s⁻¹. Errors for k_q and k_q' are estimated to be $\pm 5\%$.

Table S4. Optimum EL performance of **3**-doped OLEDs at different dopant concentrations (current density [mA cm^{-2}] in parentheses)

wt %	V_{on} [V]	L_{max} [cd m^{-2}]	$\eta_{ext,max}$ [%]	$\eta_{L,max}$ [cd A^{-1}]	$\eta_{P,max}$ [lm W^{-1}]
0.5	3.8	4 500 (753)	2.0 (9.2)	2.8 (9.2)	1.2 (9.2)
1.0	3.3	11 000 (781)	5.4 (9.5)	14 (9.5)	6.2 (9.5)
2.0	2.9	20 500 (720)	10 (8.9)	28 (8.9)	13 (8.9)
4.0	2.8	23 000 (683)	11 (8.5)	31 (8.5)	14 (8.5)
6.0	3.0	18 000 (667)	8.5 (8.0)	24 (8.0)	9.8 (8.0)

Configuration: [ITO/NPB (400 Å)/CBP:**3** (x wt %) (300 Å)/BCP (200 Å)/Alq₃ (300 Å)/LiF (5 Å)/Al (1500 Å)]

Table S5. EL performance of **1**-doped OLEDs at different dopant concentrations (configuration: [ITO/NPB (500 Å)/Bepp₂:**1** (x wt %) (500 Å)/LiF (15 Å) /Al (1500 Å)])

Device	Conc. of 1		EL Color	L [a]	η_P [a]	Max. L [cd m ⁻²]	Max. η_P [lm W ⁻¹]	Max. η_{ext} [%]
	[wt %]	CIE (x, y)		[cd m ⁻²]	[lm W ⁻¹]	(Current density [mA cm ⁻²])	(Current density [mA cm ⁻²])	
A	3.2	0.33, 0.35	white	451	0.79	3044 (307)	0.85 (13)	1.1
B	7.7	0.37, 0.41	yellow	737	1.20	3246 (166)	1.47 (3)	1.6
C	11.1	0.43, 0.47	yellow	800	1.43	2812 (110)	1.61 (11)	1.5
D	16.7	0.45, 0.48	yellow	629	1.00	2609 (209)	1.13 (7)	1.3

[a] At 20 mA cm⁻².